Control and Performance Analysis of a Single-Stage Utility-Scale Grid-Connected PV System

Vivek Nandan Lal, *Student Member, IEEE*, and S. N. Singh, *Senior Member, IEEE*

***Abstract*—For utility-scale photovoltaic (PV) systems, the control objectives, such as maximum power point tracking, synchronization with grid, current control, and harmonic reduction in output current, are realized in single stage for high efficiency and simple power converter topology. This paper considers a high-power three-phase single-stage PV system, which is connected to a distribution network, with a modified control strategy, which includes compensation for grid voltage dip and reactive power injection capability. To regulate the dc-link voltage, a modified voltage controller using feedback linearization scheme with feed-forward PV current signal is presented. The real and reactive powers are controlled by using *dq* components of the grid current. A small-signal stability/eigenvalue analysis of a grid-connected PV system with the complete linearized model is performed to assess the robustness of the controller and the decoupling character of the grid-connected PV system. The dynamic performance is evaluated on a real-time digital simulator.**

***Index Terms*—DC-link voltage control, feedback linearization (FBL), photovoltaic (PV) systems, reactive power control, small-signal stability analysis, voltage dip.**

I. Introduction

In the past few years, penetration of power generated from the photovoltaic (PV) systems into the electricity grid has been considerably increasing due to the advancement in technology leading to the cost reduction of the power electronic device and many incentive programs introduced by the governments [1]. In the grid-connected PV systems, the most important aims are to reduce cost and improve efficiency and reliability of both the PV panels and converters [2], [3]. To achieve these, single-stage three-phase dc-to-ac power converter system seems to be the best choice for utility-scale high-power PV system [4]. The continuous increase in the interconnection of these megawatt-sized PV systems in the distribution network requires study of PV system impacts on the distribution network and performance of controllers under steady-state and dynamic conditions.

Manuscript received January 7, 2014; revised May 15, 2014, August 14, 2014, and October 12, 2014; accepted February 21, 2015. Date of publication March 25, 2015; date of current version September 27, 2017.

V. N. Lal is with the Department of Electrical Engineering, Indian Institute of Technology, Kanpur 208 016, India, and also with the Department of Electrical Engineering, Indian Institute of Technology (Banaras Hindu University), Vanarasi 221 005, India (e-mail: vnlal.eee@itbhu.ac.in).

S. N. Singh is with the Department of Electrical Engineering, Indian Institute of Technology, Kanpur 208 016, India (e-mail: snsingh@iitk.ac.in).

Digital Object Identifier 10.1109/JSYST.2015.2408055

The dynamic behavior of PV system is characterized by its system architecture, control techniques, distribution network parameters, and weather conditions. Much literature have discussed about these aspects previously. References [5]–[7] suggested different power electronic converter topologies for distributed generation. A survey of maximum power point tracking (MPPT), the most common aspect in PV system, is thoroughly discussed in [8] and [9]. However, most of the previous work have investigated about two-stage PV system. Only few references have considered the control aspects with both the active and reactive powers and stability for single-stage utility-scale (high-power) PVs. References [10]–[13] investigate control strategies for single-stage PV system without stability consideration. Reference [10] highlights the current and voltage control issues but does not discuss about grid connection and reactive power control. In [11], PV system as reactive power ancillary service is proposed. Yazdani *et al.* [12] presented the modeling guidelines for simulation study of grid-connected PV system utilizing power signal for forward compensation in voltage controller, but dynamic model and stability aspects are not attempted. In [13], a feedback linearization (FBL) technique is used in combined form for both current and voltage controllers, which increase the design complexity and oscillations in the dc voltage during MPPT control.

Reference [14] has performed eigenvalue analysis to evaluate dynamic behavior of PV system in a two-stage topology. In [15], two models for PV system are proposed, and based on these models, system voltage and angle stability of grid-connected PV system have been analyzed without MPPT dynamics. Du *et al.* [16] have investigated the effect of large-scale PV penetration on small-signal stability for two-stage three-phase inverter topology. Reference [17] has discussed analysis and control of PV system integrated with IEEE 14-bus system, utilizing two-stage power conversion topology. In [18], control strategy similar to [12] is used, and sensitivity analysis is performed with distribution network modeled as an RLC circuit in PSCAD environment. The control strategy for voltage controller used in this paper is different and is based on FBL technique with voltage signal as the input reference and the feedback signal of controller, whereas in [18], the square of voltage signal is used for that purpose, which increases the complexity of the controller design. Furthermore, to the best of the authors' knowledge, the controller performance and dynamic stability analysis of a utility-scale (single-stage) PV system integrated with a standard-size distribution network has not been attempted.

This paper investigates the performance of a utility-scale PV system connected to a distribution system with a modified

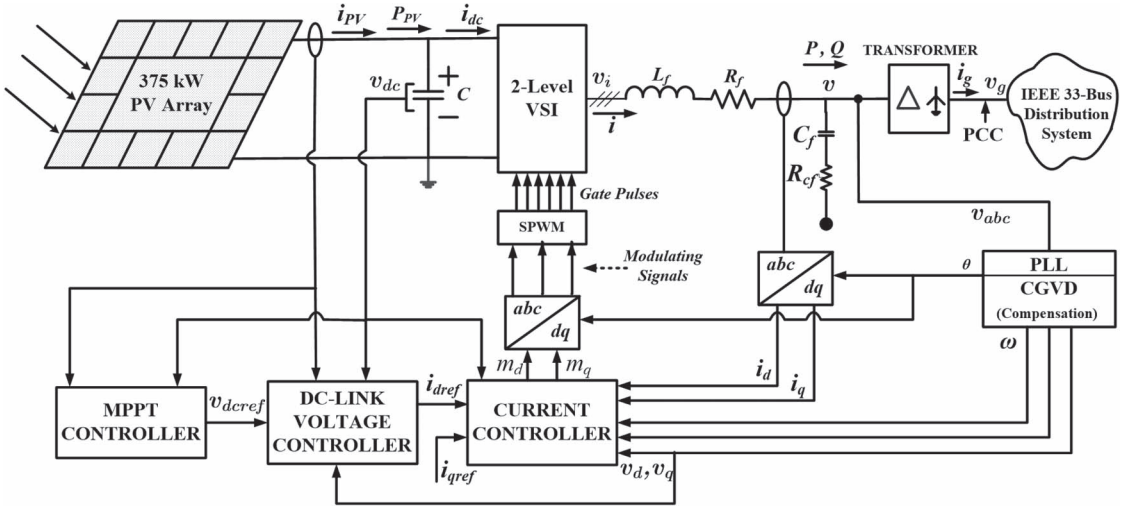

Fig. 1. One of the four 375-kW subsystems.

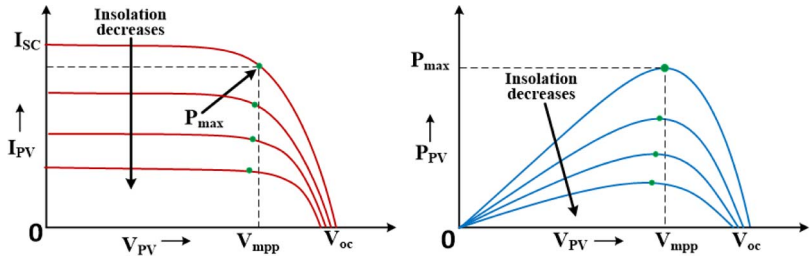

Fig. 2. PV array current and power output characteristics.

control strategy. The major contributions of the this work are as follows.

- For active power control with incremental conductance MPPT method, a simple and linearized dc-link voltage controller with FBL technique and d-axis current control are used, whereas for reactive power control, a q-axis current controller is used.
- For voltage controller design, FBL scheme is used to avoid the impacts of distribution network parameters variation and the nonlinearity caused by the PV characteristics.
- Unlike the control scheme used in [13], FBL technique is used in this work only for voltage controller to make the controller simple with improved results.
- The overall control scheme has been modified and improved with a proposed additional block for compensation for grid voltage disturbance/dip (CGVD) to avoid the destabilization of controllers.

A linearized model is used to examine the dynamic behavior of the PV system with controllers using eigenvalue analysis. Parallel operation of four PV units sequentially connected to a grid is also conducted, and short-circuit fault is applied to test the stability of the system. The performance of the PV system with the proposed controllers is tested on an IEEE 33-bus distribution system.

This paper is organized into various sections as follows. A brief description of the overall system architecture under analysis is provided in Section II; Section III presents the main features of various control schemes; Section IV describes the mathematical dynamic modeling of the PV system connected to an IEEE 33-bus distribution network; Section V discusses the eigenvalue analysis of the steady-state and dynamic performance of the system based on a linearized model; simulation results are discussed in Section VI, and finally, conclusions are drawn in Section VII.

II. PV System Architecture

Fig. 1 shows a single-stage three-phase PV system connected to an IEEE 33-bus distribution grid. The complete PV system (375 kW) consists of many structural units such as PV array; a three-phase two-level six-pulse pulsewidth modulated voltage source inverter (VSI) with a switching frequency of 6 kHz; a low-pass filter; and the transformer connected with the utility grid at a point of common coupling (PCC). The 375-kW PV array is realized by using series–parallel combination of 150-W modules (25 in series and 100 in parallel). The characteristics of a typical PV array are shown in Fig. 2. It is shown that, at zero voltage, power output is zero and the current is maximum termed as short-circuit current for a particular insolation. The power increases with the voltage up to a certain maximum power point (MPP). Then, power and current both decrease until zero at open-circuit voltage.

The PV array is connected to the dc side of the VSI with a dc-link capacitor. The control of this VSI is based on sinusoidal pulsewidth modulation. The ac side of the inverters is

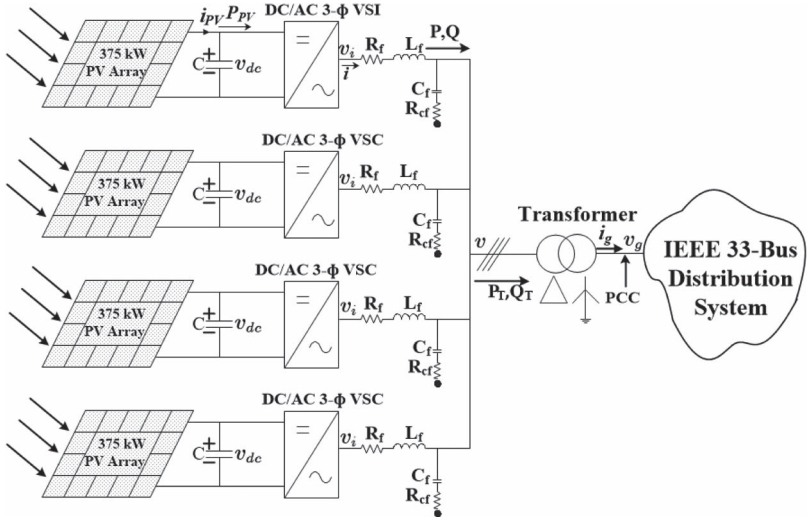

Fig. 3. Overall 1.5-MW system architecture.

connected to the harmonic filters. The series branch of the filter consists of an inductor, and the shunt branch is having delta connected capacitors in series with resistance. By combining several numbers of such PV systems in parallel, larger capacity PV systems can be formed, as shown in Fig. 3, where a three-phase single-stage 1.5-MW PV system is realized by using four 375-kW systems.

III. Control Schemes

The control schemes for grid synchronization, MPPT, dc-link voltage control, and real and reactive power controls are presented in the following subsections.

A. Grid Synchronization

For PV system synchronization with grid, the amplitude and phase angle of the utility grid voltage are identified. A synchronous reference frame approach based conventional phase-locked loop (PLL) [19] with a proposed modified block is used. This modified block is a compensator for grid voltage disturbance (CGVD). The d- and q-axes components v_d and v_q of the grid voltage v_{abc} are passed through a compensator block and used in the PLL scheme. By setting the q-axis voltage component equal to zero, the PLL angle θ is made equal to the phase angle of the grid phase voltage v_a, as shown in Fig. 4. The PLL gives much improved results by using filtered voltage in terms of fluctuations in the d- and q-axes voltages, which, consequently, improves the performance of the other controllers.

B. Compensator for Grid Voltage Dip

Voltage dip phenomena in a power system are caused by three main reasons: nonlinear load connection, sudden connection of large loads, and short-circuit faults. Due to sudden voltage dips, problems in control of PV system can arise, such as possibility of unstable operation of controller, dc-side voltage oscillations, and distortion in ac currents. According to

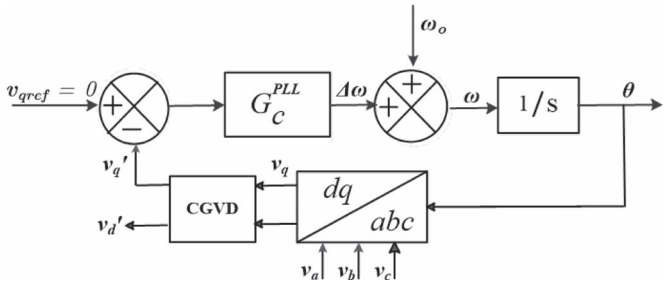

Fig. 4. PLL control scheme.

European Standard EN 50160, the voltage dips can be classified as follows [20]:

- shallow (below 60%) and long (above few seconds);
- deep (more than 60%) and long;
- shallow (below 60%) and short (up to few seconds);
- deep (more than 60%) and short.

There are different types of voltage dips, e.g., three-phase voltage dip, single-phase voltage dip, two-phase voltages dip, and change in phase shift. These voltage dips generate the zero- and negative-sequence components at grid side. As the dq components of the grid-side voltage and current are one of the key components of control strategy, a compensator for grid voltage dip is designed by including filters in the PLL control scheme, which is shown in Fig. 5. In the case of voltage dip, the negative-sequence component of voltage in the dq component appears as 100-Hz notches, which have to be separated and eliminated from control and synchronization blocks. Moreover, the dq transformed grid voltage on the ac side of the inverter contains high frequency harmonics. Therefore, proper filtering is used to filter out the 100-Hz notches and other harmonics. The d- and q-axes grid voltages are passed through a band reject filter of 100 Hz to filter out the notches along with a low-pass filter of 75 and 150 Hz for d- and q-axes voltages, respectively. These low-pass filter values are the rough estimates and decided by heuristic approach as there are higher harmonics visible in

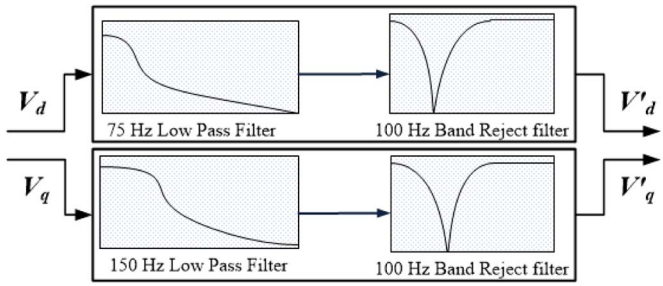

Fig. 5. Compensator for grid voltage dip (CGVD).

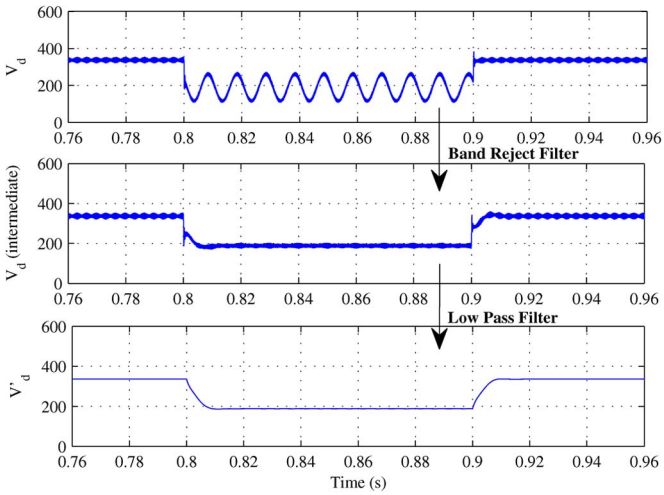

Fig. 6. d-Axis voltage filtering process in case of voltage dip.

the dq components, and these low-pass filters are very much appropriate to give the satisfactory filtering response of almost all harmonics. By doing this, the dynamic performance of the controllers is improved. The filtering process of the d-axis voltage component is shown in Fig. 6.

The filtering process may be achieved by using the sequence analysis. However, to implement that analysis in simulation, voltages have to be converted into the positive and negative sequences and then filtering is done, and then, again, it is to be converted into dq-axis for the other controller purpose. Therefore, extra process is added. In this work, the filter is being applied directly to the dq components of voltage after $abc{-}dq$ transformation, which simplifies the process and reduces the computational burden without compromising the accuracy.

C. MPPT Algorithm

It is evident from the PV characteristics (see Fig. 2) that the PV array has a single operating terminal voltage, only for which the array delivers maximum power at a particular insolation and temperature. The aim of MPPT is to track the MPP irrespective of variations in atmospheric conditions. The most popular MPPT algorithms presented in the literature are the perturb and observe (P&O) and incremental conductance (INC) methods [9]. The P&O method is simple in implementation but has limitations with rapidly changing atmospheric conditions and may not work correctly in some cases. Therefore, in this paper, the INC method is considered to track the MPP.

D. DC-Link Voltage Control

The dc-link voltage controller presented in this paper is based on FBL technique [21]. The controller is used to regulate the dc-link capacitor voltage according to the reference voltage v_{dcref}, which is decided by the MPPT scheme. The dc-link voltage regulation is achieved through the control of direct axis current, which, consequently, controls the real power injection into the grid. Fig. 7 shows the dc-link voltage control scheme, which is designed on the basis of the FBL technique. Neglecting the inverter power loss, according to the power balance of both sides of the inverter in steady state, P_{PV} should be equal to the power output of the VSI ac-side terminals, which is equal to the output grid power P, ignoring the filter power loss. The controller works on the voltage dynamics of dc-link capacitor based on power balance principle, as given by

$$\frac{d}{dt}\left(\frac{1}{2}Cv_{\mathrm{dc}}^2\right) = P_{\mathrm{PV}} - P. \tag{1}$$

This can be simplified as

$$C\frac{dv_{\mathrm{dc}}}{dt} = i_{\mathrm{PV}} - \frac{3}{2}\frac{v_d}{v_{\mathrm{dc}}}i_d \tag{2}$$

where v_d and i_d are the d-axis grid voltage and current, respectively; and $P = (3/2)v_d i_d$ [22]. Equation (2) is a nonlinear differential equation, as it is clear from the PV characteristic that i_{PV} is a nonlinear function of $v_{\mathrm{PV}}(= v_{\mathrm{dc}})$ and it is linearized using FBL.

According to the FBL technique [23], if $f(x)$ and $b(x)$ are nonlinear functions of a system with states x, as

$$\dot{x} = f(x) + b(x) * u_i \tag{3}$$

using the control input u_i as

$$u_i = \frac{1}{b}[u_v - f] \tag{4}$$

the nonlinearities can be cancelled out as

$$\dot{x} = u_v. \tag{5}$$

Considering i_d $(= (2/3)(v_{\mathrm{dc}}/v_d)[i_{\mathrm{PV}} - u_v])$ as a control input, (2) can be written in the form of a linear differential equation as

$$C\frac{d}{dt}(v_{\mathrm{dc}}) = u_v. \tag{6}$$

From (6), a plant transfer function is derived as

$$G_p(s) = \frac{v_{\mathrm{dc}}(s)}{u_v(s)} = \frac{1}{sC}. \tag{7}$$

For the preceding plant transfer function, a PI controller $G_c^{v_{\mathrm{dc}}}$ is designed with proper phase margin and settling time, which is ten times of that of the current controller. Due to this difference

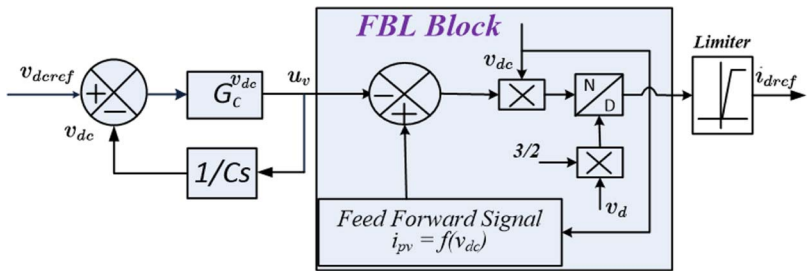

Fig. 7. Block diagram of the dc-link voltage control.

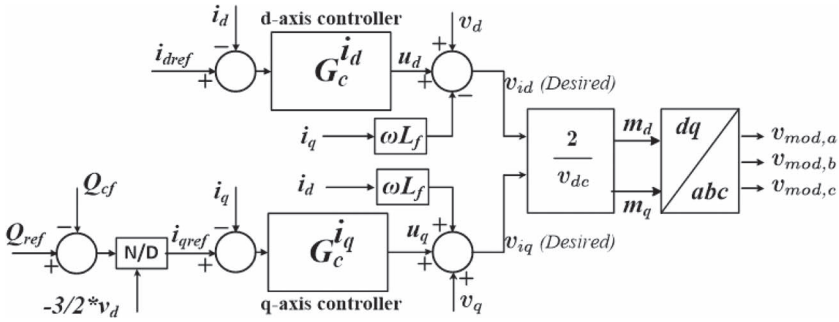

Fig. 8. Complete real and reactive power control scheme (d- and q-axes current control).

in settling time, decoupling feature is introduced in the voltage and current controllers.

For the aforementioned FBL technique, there is a singular point $b(x) = 0$ or close to zero, which makes the system unstable. This happens when v_d is close to zero, which is possible only in the case of three phase lines to ground (LLLG) fault with very small resistance, which is rare in power system.

E. Real and Reactive Power Control/AC Current Control

The real and reactive powers are controlled by using current-mode control approach of VSI by controlling the d- and q-axes components of grid currents, respectively [12], by using PI controllers (see Fig. 8). With MPPT, the d-axis current control is linked with the dc-link voltage regulation. The dc-link voltage controller output $i_{\rm dref}$ is used as reference for real power controller. $i_{\rm qref}$ is calculated by using the formula $Q = -(3/2)v_d i_q$ [22]. The reactive power delivered by the shunt branch of the filter, i.e., Q_{cf}, is compensated by subtracting it from $Q_{\rm ref}$. The current controllers generate sinusoidal modulating signals and control the output voltage, i.e., v_i, of the VSI, which, in turn, control the grid current, and accordingly, powers are controlled.

IV. System Modeling for Small-Signal Analysis

In order to understand the dynamic behavior of a grid-connected PV system with modified controller, a small-signal analysis is carried out using the linearized model of the PV system and the electric grid. To obtain the linearized models, the dynamic equations of the PV system along with its controllers and distribution network are to be derived. The following subsections explain the modeling of the different segments of the PV system connected to the distribution system.

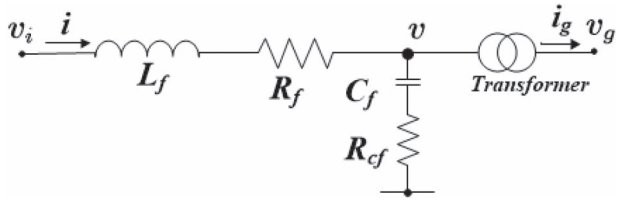

Fig. 9. Filter branch and transformer.

A. PV Circuit

The PV circuit includes a dc-link capacitor, a series filter (inverter ac current dynamics), the shunt branch of the filter, and transformer impedance. The dynamics in the dc-link capacitor defined by (2) in Section III-D give the state variable $v_{\rm dc}$. Fig. 9 shows the filters and the transformer. The mathematical model of the dynamics of inverter ac current in the series filter is defined by the following equations in dq frame:

$$L_f \frac{di_d}{dt} = -R_f i_d + \omega L_f i_q + v_{id} - v_d \tag{8}$$

$$L_f \frac{di_q}{dt} = -R_f i_q - \omega L_f i_d + v_{iq} - v_q. \tag{9}$$

The dynamics of the shunt branch of the filter and the transformer impedance are given by

$$C_f \frac{dv}{dt} = i - N i_g + C_f R_{cf} \left(\frac{di}{dt} - \frac{di_g}{dt} \right) \tag{10}$$

$$L_T \frac{di_g}{dt} = -R_T i_g + N v - v_g \tag{11}$$

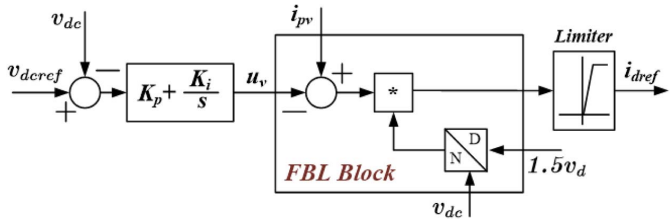

Fig. 10. DC-link voltage controller block diagram.

where N, L_T, and R_T are the turn ratio, the inductance, and the resistance of the transformer, respectively. i_g and v_g are the grid injected current and PCC voltage, respectively. State variables i_d and i_q are defined by (8) and (9), v_d and v_q by (10), and i_{gd} and i_{gq} by (11).

B. DC-Link Voltage Controller

The dc-link voltage controller is designed using the FBL technique as discussed in Section III-D. The detailed control block diagram is shown in Fig. 10. From the dc-link voltage controller, i_{dref} is given to the current controller. The time-domain equation describing the voltage controller dynamics can be given as

$$\frac{du_v}{dt} = K_i(v_{\mathrm{dcref}} - v_{\mathrm{dc}}) + K_p\left(\frac{dv_{\mathrm{dref}}}{dt} - \frac{dv_{\mathrm{dc}}}{dt}\right) \tag{12}$$

where u_v is the state variable, v_{dcref} is the reference signal for the voltage controller from the MPPT controller, and K_p and K_i are the proportional and integral gains of the PI controller used in the voltage controller.

C. Current Controller

To generate the modulating signals for VSI, the proposed dq-axis current control strategy is discussed in Section III-D (see Fig. 8). From the current controller, the output voltage signals (v_{id} and v_{iq}) for the inverter are obtained. In modeling of the current controller, the inverter is considered as a unity gain block, and the time delay caused by the inverter to produce the output voltage signals is neglected. The equations describing the dynamics of the d- and q-axes current controllers in time domain are derived as

$$\frac{dv_{id}}{dt} = K_P\left(\frac{di_{\mathrm{dref}}}{dt} - \frac{di_d}{dt}\right) + K_I(i_{\mathrm{dref}} - i_d) + \frac{dv_d}{dt} - \omega L\frac{di_q}{dt} - Li_q\frac{d\omega}{dt} \tag{13}$$

$$\frac{dv_{iq}}{dt} = -K_P\frac{di_q}{dt} - K_I i_q + \frac{dv_q}{dt} + \omega L\frac{di_d}{dt} + Li_d\frac{d\omega}{dt} \tag{14}$$

where v_{id} and v_{iq} are the state variables. K_P and K_I are the proportional and integral gains of the PI controllers ($G_c^{i_d}$ and $G_c^{i_q}$).

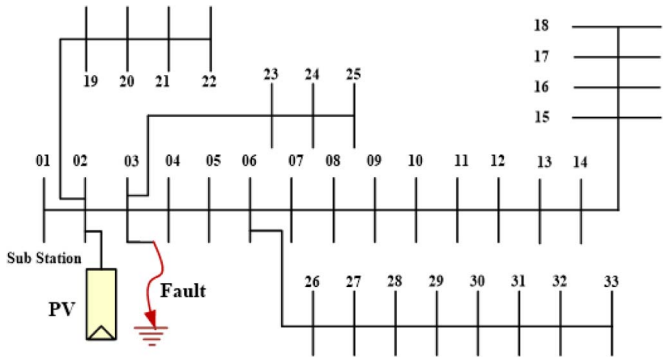

Fig. 11. IEEE 33-bus distribution network connected with a PV plant.

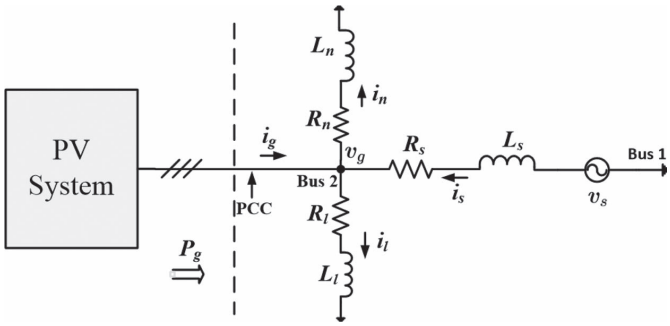

Fig. 12. PV system integration with equivalent distribution network.

D. PLL Controller

For mathematical modeling, the equation describing the PLL (see Fig. 4) is given as

$$\frac{d\theta}{dt} = \omega. \tag{15}$$

In the modified PLL control structure used in this paper, the q-axis component of the transformer's primary side voltage v_q is passed to a low-pass filter having time constant τ, and the output v_q' can be written as

$$\frac{dv_q'}{dt} = \frac{1}{\tau}\left[v_q - v_q'\right]. \tag{16}$$

Therefore, the dynamic equation describing PLL control logic can be given by

$$\frac{d\omega}{dt} = -k_p\frac{dv_q'}{dt} - k_i v_q' \tag{17}$$

where k_p and k_i are the proportional and integral gains of the PI controller, respectively; and ω, θ, and v_q' are the state variables of the PLL.

E. Distribution System

The PV system with a local load (R_l is series with L_l) is connected at bus 2 of the IEEE 33-bus distribution system, as shown in Fig. 11. Kron's reduction technique is used [24] to obtain the equivalent reduced network of the distribution network for linearized analysis.

Fig. 12 shows the single-line representation of the PV system interfaced with reduced distribution network, where buses 1 and

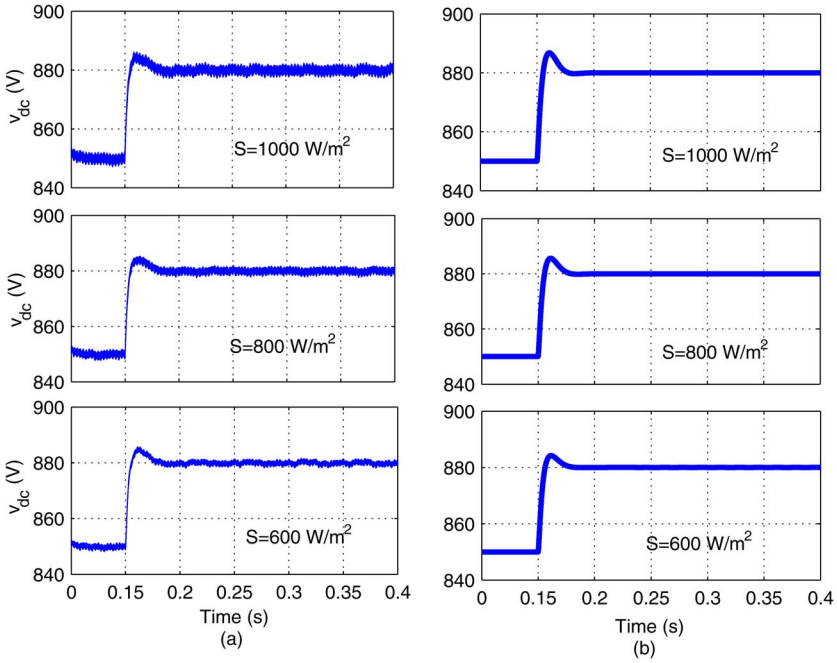

Fig. 13. $v_{\rm dc}$ response at different insolation levels from the (a) RSCAD model and the (b) linearized system model.

2 are retained and the rest of the buses are eliminated. R_n and L_n represent the equivalent network, and R_l and L_l represent the local load at the retained bus 2. R_s and L_s represent the network between the distribution substation (which is represented by an ideal voltage source) and the retained bus. P_g is the power injected into the distribution network. i_n, i_l, and i_s are the network current, the load current, and the substation current, respectively. At PCC, where the transformer is connected to the distribution network, the local load and network impedances, which are in parallel, are combined to form an equivalent impedance (L_{nl} in series with R_{nl}), and equivalent current i_{nl} (sum of i_n and i_l) flows in this branch. The dynamics of the distribution network are described in dq frame as

$$L_{nl}\frac{di_{nld}}{dt} = -R_{nl}i_{nld} + \omega L_n l i_{nlq} + v_{gd} \tag{18}$$

$$L_{nl}\frac{di_{nlq}}{dt} = -R_{nl}i_{nlq} - \omega L_n l i_{nld} + v_{gq} \tag{19}$$

$$L_s\frac{di_{sd}}{dt} = -R_s i_{sd} + \omega L_s i_{sq} + v_{sd} - v_{gd} \tag{20}$$

$$L_s\frac{di_{sq}}{dt} = -R_s i_{sq} - \omega L_s i_{sd} + v_{sq} - v_{gq} \tag{21}$$

where i_{nld}, i_{nlq}, i_{sd}, and i_{sq} are the state variables of the distribution network; and v_{gd} and v_{gq} are the d- and q-axes of the PCC voltage v_g, respectively.

V. Eigenvalue Analysis

The linearized equations of the overall system defined by (2) and (8)–(21) can be written in state-space form as [25]

$$\tilde{\dot{\mathbf{x}}}_{\rm sys} = \mathbf{A}_{\rm sys}\tilde{\mathbf{x}}_{\rm sys} + \mathbf{B}_{\rm sys}\tilde{\mathbf{u}}_{\rm sys} \tag{22}$$

where $\tilde{\mathbf{x}}_{\rm sys}$ is a state vector that consists of 17 state variables (13 for PV system and 4 for distribution system). $\mathbf{A}_{\rm sys}$ and $\mathbf{B}_{\rm sys}$ are the plant and control matrices, respectively, and the input vector is

$$\tilde{\mathbf{u}}_{\rm sys} = [\tilde{v}_{\rm dcref} \quad \tilde{S} \quad \tilde{i}_{\rm qref}] \tag{23}$$

where $\tilde{v}_{\rm dcref}$, $\tilde{S}$, and $\tilde{i}_{\rm qref}$ are perturbations in reference dc voltage, insolation, and reference reactive power, respectively.

Thus, the overall system consists of 17 eigenvalues, each one corresponds to a system mode. To evaluate the accuracy of the linearized model, a perturbation is applied to the system around steady-state condition, and results obtained from MATLAB are compared with those of the actual model (PV system with full distribution system) implemented in RSCAD. The model accuracy is evaluated at three steady-state operating points (insolation $S = 1000$, 800, and 600 W/m^2), with $v_{\rm dcref}$ and $i_{\rm qref}$ at 850 V and 0 A, respectively.

At $t = 0.15$ s, a 30-V step change in $v_{\rm dcref}$ is applied. Fig. 13(a) and (b) illustrates the dc-voltage, i.e., $v_{\rm dc}$, response of the simulated RSCAD model and the linearized model in MATLAB at different insolation levels. In Fig. 13, it is shown that the linearized model gives almost the same response as the RSCAD model. Thus, the validity of the linearized model is established.

An eigenvalue analysis is performed on the linearized model of the system represented by (22). Table I shows the eigenvalues λ_1 to λ_{17} of the overall system at steady-state operating point of $v_{\rm dc}$ equal to 850 V, which is a solution of $|\mathbf{A}_{\rm sys} - \lambda\mathbf{I}| = 0$. λ_1 to λ_{13} belong to the PV system, and λ_{14} to λ_{17} belong to the distribution network. Since all the eigenvalues are in the left half of the s-plane, the system is stable. Table I also shows the state variables of the whole system and the participation factor

TABLE I
PARTICIPATION MATRIX AND EIGENVALUES OF THE OVERALL SYSTEM

State variables of overall system	i_d	i_q	v_{id}	v_{iq}	v_{dc}	u_v	v'_{sq}	ω	θ	v_d	v_q	i_{gd}	i_{gq}	i_{nld}	i_{nlq}	i_{sd}	i_{sq}
$\lambda_1 = -636$	1.428	0	0.303	0	0.099	0.236	0	0	0	0.354	0	0.004	0	0	0	0	0
$\lambda_2 = -218$	0	1.007	0	0.004	0	0	0	0	0	0	0.003	0	0	0	0	0	0
$\lambda_3 = -2899$	0.289	0	1.407	0	0.004	0.017	0	0	0	0.126	0	0.005	0	0	0	0	0
$\lambda_4 = -2459$	0	0.007	0	1.103	0	0	0	0.003	0	0	0.086	0	0	0	0	0	0
$\lambda_{5,6} = -84 \pm 97i$	0.139	0	0.009	0	0.506	0.632	0	0	0	0	0	0.001	0	0	0	0	0
$\lambda_7 = -66$	0	0	0	0	0	0	1.206	0.103	0.103	0	0	0	0	0	0	0	0
$\lambda_{8,9} = -265 \pm 550i$	0	0	0	0.015	0	0	0.535	0.610	0.608	0	0.014	0	0	0	0.002	0	0.001
$\lambda_{10,11} = -1100 \pm 24458i$	0	0	0.022	0.022	0	0	0	0	0	0.272	0.272	0.250	0.250	0	0	0	0
$\lambda_{12,13} = -1065 \pm 23704i$	0	0	0.024	0.024	0	0	0	0	0	0.274	0.274	0.250	0.250	0	0	0	0
$\lambda_{14,15} = -602 \pm 377i$	0	0	0	0	0	0	0	0	0	0	0	0	0	0.498	0.499	0.020	0.020
$\lambda_{16,17} = -2 \pm 377i$	0	0	0	0	0	0	0	0	0	0	0	0	0	0.001	0.001	0.499	0.498

TABLE II
$\lambda_{5,6}$ AT DIFFERENT OPERATING CONDITIONS

Operating condition $v_{dc}(V)$	$\lambda_{5,6}$ with FBL	$\lambda_{5,6}$ without FBL
850	-84±97i	-133±80i
900	-84±98i	-138±68i
950	-83±98i	-142±44i
1000	-52±83i	-218,-37
1050	-52±83i	-218,-34

of each state variable in particular mode corresponding to the eigenvalues.

From the table, it can be concluded that the modes corresponding to the PV system (λ_1 to λ_{13}) have insignificant participation in the network states and vice versa. Therefore, even if there is a change in the distribution network parameters during load variations, voltage sag or swell, symmetrical fault, etc., the PV system remains stable because the eigenmodes corresponding to the PV system are independent of the distribution network modes. The robust stability of the PV system is achieved due to the effective control design used in it. The critical eigenvalues in the PV system are $\lambda_{5,6}$, which belong to the dc-link voltage controller because the state variables corresponding to the dc-link voltage controller have dominant participation in $\lambda_{5,6}$. The eigenvalues λ_{10} to λ_{13} have the imaginary term, which corresponds to the resonating frequency formed by an LC filter with transformer inductance. Since these eigenvalues have a large negative real value, these oscillations are damped out very fast and do not affect the PV system dynamics.

VI. TEST RESULTS

The parameters of the complete system is given in the Appendix. The system is simulated on a real-time digital simulator (RSCAD), and MATLAB is used for the eigenvalue analysis.

A. Performance of the DC-Link Voltage Controller

Table II shows the eigenvalues of the dc-link voltage controller $(\lambda_{5,6})$ for different operating conditions with FBL block and without FBL block. With the change in operating condition, $\lambda_{5,6}$ with FBL do not change significantly compared with $\lambda_{5,6}$ without FBL. This is because the FBL linearizes the system nonlinearities introduced by the PV system at different operating points. Therefore, the response of the controller is almost same at different operating conditions, as shown in Fig. 14(c) and (d). $\lambda_{5,6}$, without FBL, have zero frequency terms for higher $v_{\rm dc}$ in their eigenmodes, which indicate that $v_{\rm dc}$ is having an overdamped response, as shown in Fig. 14(a), and an oscillatory response, as shown in Fig. 14(b). Thus, the proposed FBL control strategy maintains the consistency and cancels the effect of nonlinearities present in the PV curve under all operating conditions.

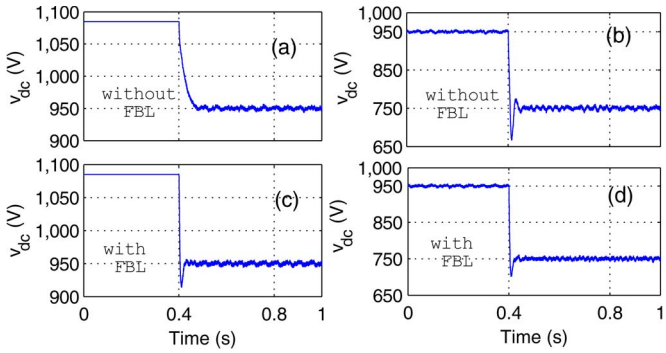

Fig. 14. v_{dc} response at different operating conditions on the PV curve.

B. MPPT and Current Controller Performance

The objective of the MPPT is to track the MPP irrespective of the operating condition and is achieved by adjusting PV array output voltage to $V_{\rm mpp}$. Fig. 15 shows the responses (PV array voltage $(v_{\rm dc})$, real power, and reactive power) of the PV system (375 kW) connected to an IEEE 33-bus distribution network. Initially, the dc-link capacitor is charged up to the open-circuit voltage of PV array, i.e., 1085 V with insolation $S = 1000\ \text{W/m}^2$, $\text{T} = 25^\circ\text{C}$, and reactive power reference $Q_{\rm ref} = 0$. The PV array real power $P_{\rm PV}$ and the grid injected reactive power (Q_g) are zero. At $t = 1$ s, MPPT is applied to the system. $v_{\rm dc}$ reaches to $V_{\rm mpp}$ (850 V) point of PV array and oscillates around it. The PV array real power $P_{\rm PV}$ increases with the decrease of the PV array voltage and becomes maximum (375 kW) at $V_{\rm mpp}$. The grid injected real power P_g also increases and becomes 350 kW at $V_{\rm mpp}$, and Q_g is still zero. The loss in

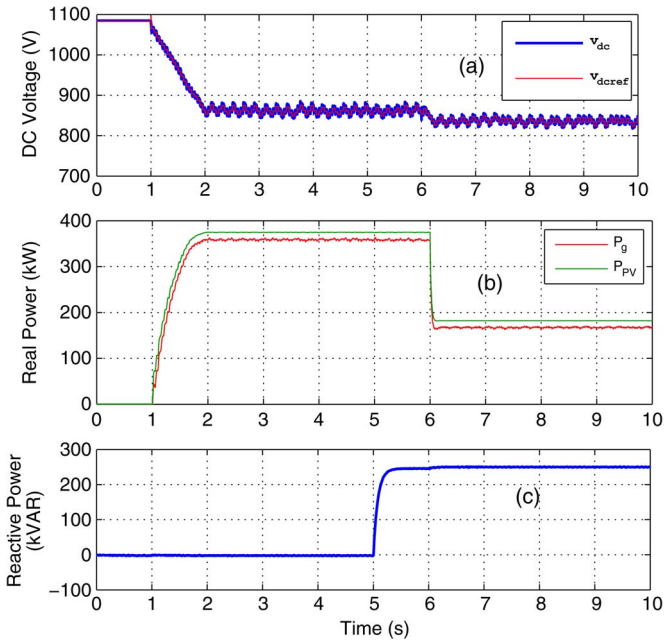

Fig. 15. (a) PV array voltage for MPPT. (b) PV array ($P_{\rm PV}$) and grid injected real power (P_g). (c) Grid injected reactive power (Q_g).

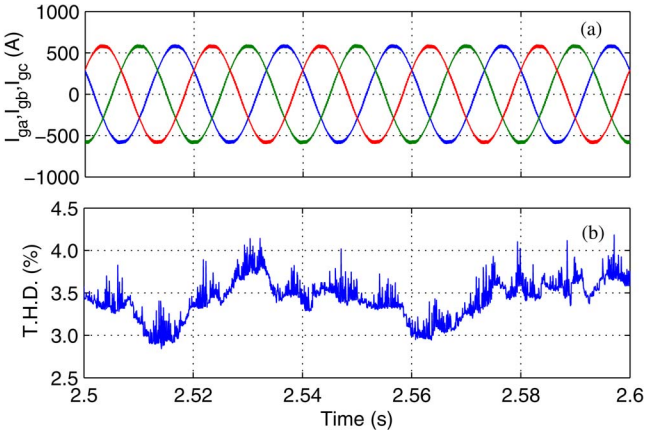

Fig. 16. Grid injected currents and THD.

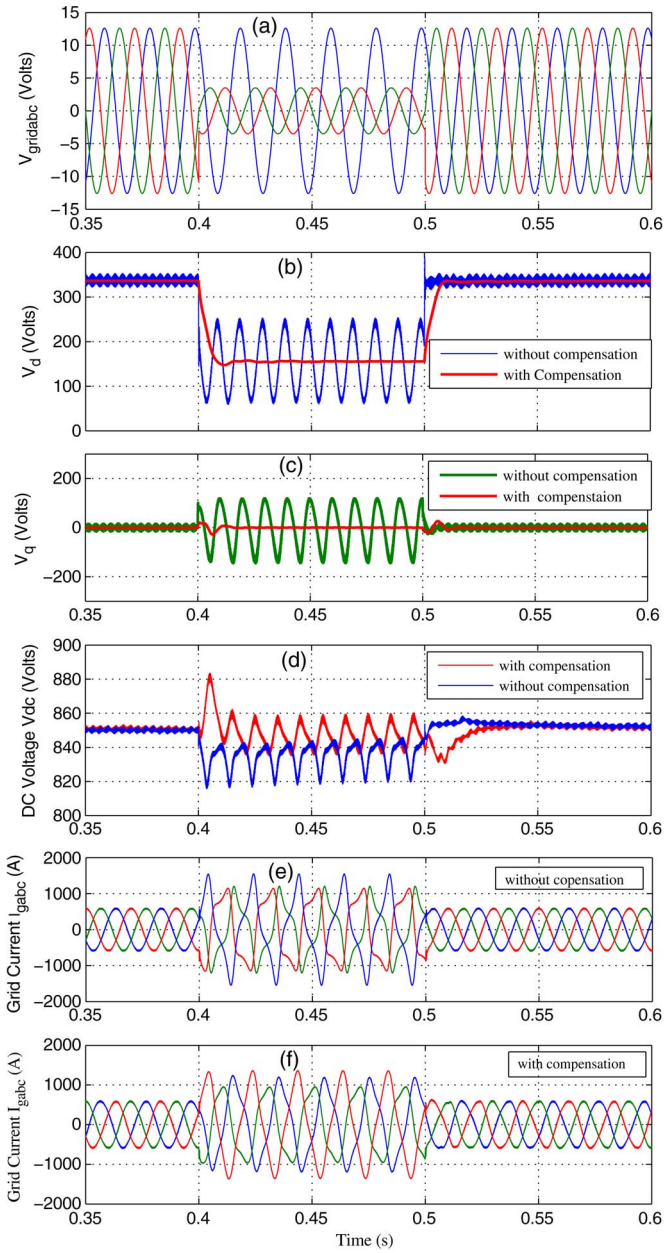

Fig. 17. PV system response to voltage dip in grid.

the inverter, resistive part of the filter, and transformer is about 25 kW (6.6%). At $t = 5$ s, reference reactive power $Q_{\rm ref}$ for the q-axis current controller is changed from 0 to 250 kVAR, and the reactive power injected to grid is changed from 0 to 250 kVAR, as shown in Fig. 15(c). There is very small (almost insignificant) disturbance in $v_{\rm dc}$ and P_g, thus showing the decoupling between the d- and q-axes current controllers.

At $t = 6$ s, a step change in insolation S from 1000 to 500 W/m^2 is applied, which changes the $V_{\rm mpp}$ of the PV curve to 830 V. The MPPT controller tracks the new $V_{\rm mpp}$ point, and $v_{\rm dc}$ oscillates around the new $V_{\rm mpp}$ according to the INC MPPT algorithm. The PV array output power $P_{\rm PV}$ decreases instantly from 375 to 182 kW (new MPP) due to sharp change in PV current $i_{\rm PV}$ (see Fig. 2), and P_g reduces to 161 kW, with losses equal to 21 kW. At this point, Q_g is disturbed very slightly, which again shows the decoupling effect between the controllers. Fig. 16(a) and (b) shows grid injected currents i_{gabc} and total harmonic distortion (THD) of grid injected current i_{ga}, for steady-state conditions at $S = 1000$ W/m^2 and $v_{\rm dc} = 850$ V from $t = 2.5$ s to $t = 2.6$ s. The THD is below 5%, which is satisfactory according to the IEEE 1547 standards [26].

C. Voltage Dip Response

The performance of the controllers for voltage dip is shown in Fig. 17. This figure shows the response of the case when there is a drop of 70% for a duration of 0.1 s (i.e., from 0.4 to 0.5 s) in voltage magnitude in two phases. Fig. 17(a) shows the three-phase grid voltages. Fig. 17(b) and (c) shows the d- and q-axes voltages, respectively, with and without compensation filters. The response of E_d and E_q is completely smoothened by the low-pass and band reject filters. This helps in the overall

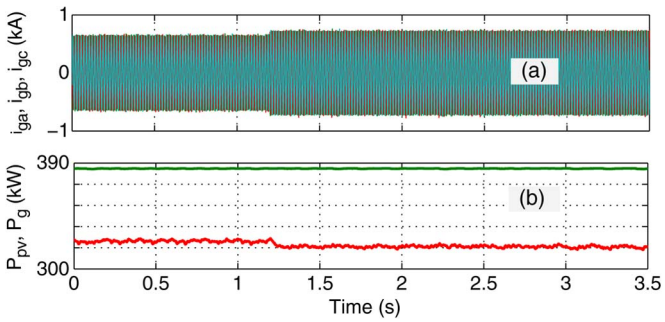

Fig. 18. PV system response to a three-phase fault at bus 3.

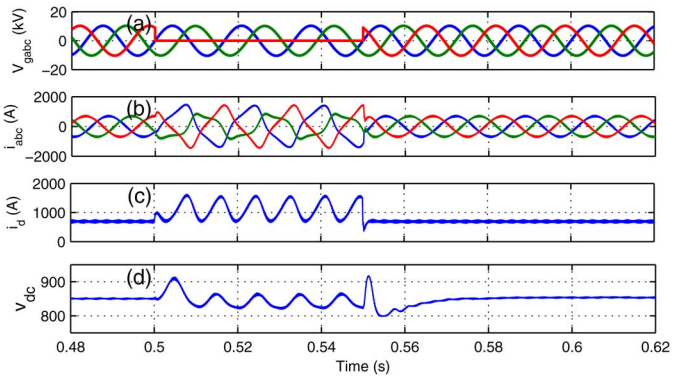

Fig. 19. PV system response to an LG fault.

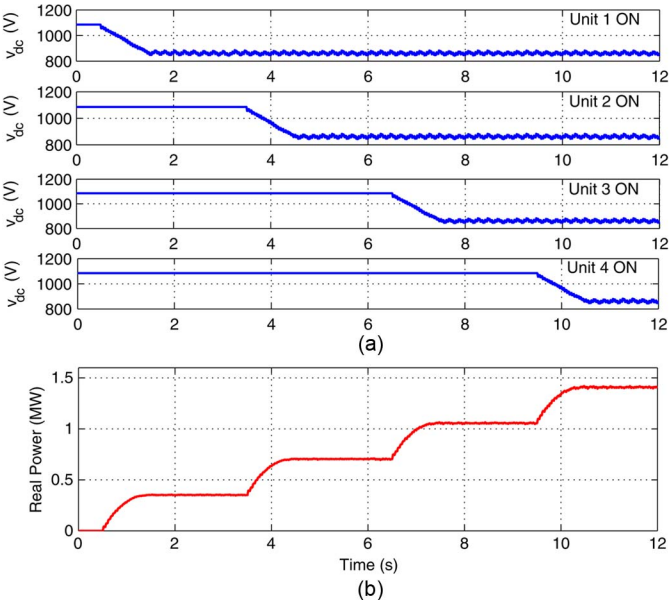

Fig. 20. P_g response of the whole 1.5-MW PV system.

performance of all interlinked controllers and prohibits the unstable operation. Fig. 17(f) shows that the distortion in grid current is also reduced compared with Fig. 17(e). In Fig. 17(d), it is clear that oscillations are present in dc voltages with and without compensation, but the average $V_{\rm dc}$ is still 850 V in compensated filtered system, whereas average $V_{\rm dc}$ is reduced to 837 V (approximately), thus reducing the real power injection to the distribution grid.

D. Three-Phase Fault

At $t = 1.2$ s, a three-phase fault is created at bus 3, as shown in Fig. 11, and the PV system stability is validated for this case. For grid currents and real power, the PV system response to a three-phase fault is shown in Fig. 18. As soon as the fault occurred, grid injected current increases because of a decrease in the PCC voltage at bus 2 to maintain the PV input and grid output power balance. There is a decrease in power P_g because of an increase in losses in inverter and filter resistance due to an increase in grid injected current.

E. LG Fault

In order to evaluate the robustness of the PV system against fault condition, a line-to-ground (LG) fault is applied to phase a on the high-voltage side of the transformer (T_r) for a duration of 50 ms from $t = 0.5$ to 0.55 s.

During the fault, the voltage of phase a is zero, and injected currents i_{abc} are also unbalanced and distorted, as shown in Fig. 19(a) and (b). Since the voltages at PCC are unbalanced and distorted, the voltage controller is affected, which introduces the fluctuations in i_d and, consequently, fluctuation in $v_{\rm dc}$, as shown in Fig. 19(c) and (d). Despite the severity of the fault, the PV system remains stable and attains to normal operation after the fault is cleared.

F. Full PV System (1.5 MW) Response

Fig. 20(a) and (b) shows the $v_{\rm dc}$ and P_g response of the system, respectively, as four numbers of 375-kW PV units are connected one by one to the system in parallel. Initially, all four units are at open-circuit condition with no controller signals. From $t = 0$ s to $t = 0.5$ s, $v_{\rm dc}$ for all the units are equal to the open-circuit voltage (1085 V), and the grid injected power P_g is zero. Controller signals for the four parallel units are given at $t = 0.5,\ 3.5,\ 6.5,$ and 9.5 s, respectively; and according to the timing sequence of controller signals, MPPT is performed to settle $v_{\rm dc}$ at $V_{\rm mpp}$ for each PV unit. Consequently, the grid injected power output P_g is changed to 350, 700, and 1050 kW and 1.4 MW with a step change of 350 kW $(= 375 - 25$ kW loss$)$.

VII. Conclusion

The proposed modified dc-link voltage controller with FBL technique, using INC MPPT, and real and reactive power controls with enhanced filter for compensation for grid voltage dips has been tested at different insolation levels on a real-time digital simulator (RTDS). Small-signal analysis of a PV system connected to an IEEE 33-bus distributed system is performed. The results from simulation and eigenvalue analysis demonstrate the effectiveness of the FBL controller compared with the controller without FBL. It is found that the FBL controller outperforms the controller without FBL, as the FBL controller's performance is linear at different operating conditions. With grid voltage dip compensator filter, the dynamic performance is much improved in terms of less oscillations and distortion

TABLE III
SYSTEM PARAMETERS

Transformer	Rated Power, Frequency	2 MVA, 50 Hz
	Voltage Rating	415 V/ 12.66 kV
	Leakage Reactance	0.05 pu
	Resistance	0.01 pu
Control Parameters	G_c^{PLL}	$k_p = 2, k_i = 120$
	$G_c^{v_{dc}}$	$K_p = 1.5, K_i = 200$
	$G_c^{i_d}$,$G_c^{i_q}$	$K_P = 0.3, K_I = 65$
PV Unit	375 kW PV System	
	V_{mpp}, I_{mpp}	850 V, 442 A
	V_{oc}, I_{sc}	1085 V, 480 A
	dc-link Capacitor	5000 F
	1.5 MW PV System	
	V_{mpp}, I_{mpp}	850 V, 1768 A
	V_{oc}, I_{sc}	1085 V, 1920 A
	dc-link Capacitor	5000 μF
Harmonic Filter	L_f, R_f	0.101mH, 0.003 Ω
	C_f, R_{cf}	186 μF, 0.225 Ω

in waveforms. In addition, the eigenvalue analysis shows that the effect of the disturbance in distribution system is negligible on PV system stability as the eigenmodes of the PV system are almost independent of the distribution system. This has been also confirmed by three-phase fault analysis of distribution system in RTDS model. The controller performance is also validated on 4×375 kW PV units connected to the distribution system.

APPENDIX

System parameters for simulation are given in Table III.

REFERENCES

[1] M. Oprisan and S. Pneumaticos, "Potential for electricity generation from emerging renewable sources in Canada," in *Proc. IEEE EIC Climate Change Technol. Conf.*, May 2006, pp. 1–10.

[2] G. Petrone, G. Spagnuolo, R. Teodorescu, M. Veerachary, and M. Vitelli, "Reliability issues in photovoltaic power processing systems," *IEEE Trans. Ind. Electron.*, vol. 55, no. 7, pp. 2569–2580, Jul. 2008.

[3] S. Jain and V. Agarwal, "A single-stage grid connected inverter topology for solar PV systems with maximum power point tracking," *IEEE Trans. Power Electron.*, vol. 22, no. 5, pp. 1928–1940, Jul. 2007.

[4] F. Katiraei and J. Aguero, "Solar PV integration challenges," *IEEE Power Energy Mag.*, vol. 9, no. 3, pp. 62–71, May-Jun. 2011.

[5] S. H. Ko, S. Lee, H. Dehbonei, and C. Nayar, "Application of voltage- and current-controlled voltage source inverters for distributed generation systems," *IEEE Trans. Energy Convers.*, vol. 21, no. 3, pp. 782–792, Sep. 2006.

[6] F. Blaabjerg, Z. Chen, and S. Kjaer, "Power electronics as efficient interface in dispersed power generation systems," *IEEE Trans. Power Electron.*, vol. 19, no. 5, pp. 1184–1194, Sep. 2004.

[7] J. Carrasco *et al.*, "Power-electronic systems for the grid integration of renewable energy sources: A survey," *IEEE Trans. Ind. Electron.*, vol. 53, no. 4, pp. 1002–1016, Jun. 2006.

[8] T. Esram and P. Chapman, "Comparison of photovoltaic array maximum power point tracking techniques," *IEEE Trans. Energy Convers.*, vol. 22, no. 2, pp. 439–449, Jun. 2007.

[9] S. Jain and V. Agarwal, "Comparison of the performance of maximum power point tracking schemes applied to single-stage grid-connected photovoltaic systems," *IET Electr. Power Appl.*, vol. 1, no. 5, pp. 753–762, Sep. 2007.

[10] R. Mastromauro, M. Liserre, and A. Dell'Aquila, "Control issues in single-stage photovoltaic systems: MPPT, current and voltage control," *IEEE Trans. Ind. Informat.*, vol. 8, no. 2, pp. 241–254, May 2012.

[11] R. Varma, B. Das, I. Axente, and T. Vanderheide, "Optimal 24-hr utilization of a PV solar system as STATCOM (PV-STATCOM) in a distribution network," in *Proc. IEEE Power Energy Soc. Gener. Meet.*, Jul. 2011, pp. 1–8.

[12] A. Yazdani *et al.*, "Modeling guidelines and a benchmark for power system simulation studies of three-phase single-stage photovoltaic systems," *IEEE Trans. Power Del.*, vol. 26, no. 2, pp. 1247–1264, Apr. 2011.

[13] F. Delfino, G. Denegri, M. Invernizzi, and R. Procopio, "A control algorithm for the maximum power point tracking and the reactive power injection from grid-connected PV systems," in *Proc. IEEE Power Energy Soc. Gener. Meet.*, Jul. 2010, pp. 1–7.

[14] L. Wang and Y.-H. Lin, "Dynamic stability analyses of a photovoltaic array connected to a large utility grid," in *Proc. IEEE Power Eng. Soc. Winter Meet.*, Jan. 2000, vol. 1, pp. 476–480.

[15] B. Tamimi, C. Canizares, and K. Bhattacharya, "Modeling and performance analysis of large solar photo-voltaic generation on voltage stability and inter-area oscillations," in *Proc. IEEE Power Energy Soc. Gener. Meet.*, Jul. 2011, pp. 1–6.

[16] W. Du, H. Wang, and R. Dunn, "Power system small-signal oscillation stability as affected by large-scale PV penetration," in *Proc. IEEE Int. Conf. SUPERGEN*, Apr. 2009, pp. 1–6.

[17] S. Balathandayuthapani, C. Edrington, S. Henry, and J. Cao, "Analysis and control of a photovoltaic system: Application to a high-penetration case study," *IEEE Syst. J.*, vol. 6, no. 2, pp. 213–219, Jun. 2012.

[18] A. Yazdani and P. Dash, "A control methodology and characterization of dynamics for a photovoltaic (PV) system interfaced with a distribution network," *IEEE Trans. Power Del.*, vol. 24, no. 3, pp. 1538–1551, Jul. 2009.

[19] G.-C. Hsieh and J. Hung, "Phase-locked loop techniques—A survey," *IEEE Trans. Ind. Electron.*, vol. 43, no. 6, pp. 609–615, Dec. 1996.

[20] "Voltage Characteristics of Electricity Supplied by Public Distribution Systems," CENELEC, Brussels, Belgium, EN-50160, 1994.

[21] V. N. Lal, M. Siddhardha, and S. N. Singh, "Control of a large scale single-stage grid-connected PV system utilizing MPPT and reactive power capability," in *Proc. IEEE Power Energy Soc. Gener. Meet.*, Jul. 2013, pp. 1–5.

[22] R. Teodorescu, M. Liserre, and P. Rodriguez, *Voltage-Sourced Converters: Modeling, Control, and Applications*. West Sussex, U.K.: Willy, 2010.

[23] E. S. Jean-Jacques and L. Weiping, *Applied Nonlinear Control*. Englewood Cliff, NJ, USA: Prentice-Hall, 1991.

[24] J. J. Grainger and W. D. Stevenson, *Power System Analysis*. Hightstown, NJ, USA: McGraw-Hill, 1994.

[25] P. Kundur, *Power system Stability and Operation*. New York, NY, USA: McGraw-Hill, 1994.

[26] *IEEE Standard for Interconnecting Distributed Resources with Electric Power Systems*, IEEE Std. 1547.2-2008, Apr. 2009.

Vivek Nandan Lal (S'13) received the B.E. degree from National Institute of Technology, Allahabad, India, in 1996 and the M.Tech. degree in electrical engineering from the Indian Institute of Technology (Banaras Hindu University) [IIT (BHU)], Varanasi, India, in 2001. He is currently working toward the Ph.D. degree in the Department of Electrical Engineering, Indian Institute of Technology, Kanpur, India.

He is also currently an Assistant Professor with the Department of Electrical Engineering, IIT (BHU).

S. N. Singh (M'01–SM'02) received the M.Tech. and Ph.D. degrees from the Indian Institute of Technology Kanpur, Kanpur, India, in 1989 and 1995, respectively.

He is currently working as a Professor with the Department of Electrical Engineering, Indian Institute of Technology Kanpur. His research interests include power system restructuring, power system optimization and control, voltage security and stability analysis, renewable energy power conversion system, distributed generation, microgrid, and artificial neural network application to power system problems.

Prof. Singh is a Fellow of The Institution of Engineers (India), The Institution of Electronics and Telecommunication Engineers (India), and The Institution of Engineering and Technology (U.K.).